A new perspective on the diffuse gamma-ray emission excess*

En-Sheng Chen (陈恩生)[1,2†] Kun Fang (方堃)[1‡] Xiao-Jun Bi (毕效军)[1,2§]

[1]Key Laboratory of Particle Astrophysics, Institute of High Energy Physics, Chinese Academy of Sciences, Beijing 100049, China
[2]University of Chinese Academy of Sciences, Beijing 100049, China

Abstract: The Large High-Altitude Air Shower Observatory (LHAASO) recently published measurements of diffuse Galactic gamma-ray emission (DGE) in the 10−1000 TeV energy range. The measured DGE flux is significantly higher than the expectation from hadronic interactions between cosmic rays (CRs) and the interstellar medium. This excess has been proposed to originate from unknown extended sources produced by electron radiation, such as pulsar wind nebulae or pulsar halos (PWNe/halos). In this paper, we propose a new perspective to explain the DGE excess observed by LHAASO. The masking regions used in the LHAASO DGE measurement may not fully encompass the extended signals of *known* PWNe/halos. By employing a two-zone diffusion model for electrons around pulsars, we find that the DGE excess in most regions of the Galactic plane can be well explained by the signal leakage model under certain parameters. Our results indicate that this signal leakage from known sources and contributions from unresolved sources should be considered as complementary in explaining the DGE excess.

Keywords: cosmic rays, diffuse gamma-ray emission, pulsar wind nebulae, pulasr halos, two-zone diffusion

DOI: 10.1088/1674-1137/ad72d4

I. INTRODUCTION

The diffuse Galactic gamma-ray emission (DGE) is crucial for studying the origin and propagation of cosmic rays (CRs). Traditionally, the DGE from the Galactic plane is believed to be dominantly generated by the interactions between the propagating CRs and interstellar medium (ISM) [1, 2]. However, in the TeV-PeV energy range, the DGE predicted by the CR-ISM interaction model is significantly lower than those observed by Milagro, ARGO-YBJ, and the Tibet AS+MD array [3−5], which is known as the TeV DGE excess [6, 7].

Recently, the Large High-Altitude Air Shower Observatory (LHAASO) published the gamma-ray source catalog of the TeV-PeV energy band [8] and the measurement of DGE in the 10−1000 TeV energy range by masking the source regions [9]. The measured DGE flux in the inner Galaxy region is approximately 3 times higher than the expectation from the CR-ISM interactions and approximately 2 times higher than that expected in the outer Galaxy region [10]. Meanwhile, neutrinos are produced alongside gamma rays during the CR-ISM interactions. The IceCube neutrino telescope has measured the high-energy neutrino flux from the Galactic plane in the energy range of 1−100 TeV [11]. Subtracting possible contribution of point sources from the total neutrino measurement and applying the masking method of LHAASO, Ref. [12] argued that the gamma-ray flux associated with the neutrino flux is consistent with that predicted by the CR-ISM interactions. This result supports that the TeV DGE excess is mainly contributed by leptonic processes[1)].

In the LHAASO DGE measurement, each source region is masked with a 2.5 times Gaussian width of the source. For point and Gaussian-like sources, this method can effectively remove the source contamination to the DGE. However, the morphology of pulsar wind nebulae (PWNe) and pulsar halos can be extended further than the Gaussian distribution. Spatially-dependent transport of electrons and positrons[2)], such as two-zone diffusion, is suggested for these systems [13, 14], indicating that there could be more gamma-ray signals than predicted by the

Received 22 July 2024; Accepted 23 August 2024; Published online 24 August 2024

* Supported by the National Natural Science Foundation of China (12105292, 12175248, 12393853)

† E-mail: chenes@ihep.ac.cn
‡ E-mail: fangkun@ihep.ac.cn
§ E-mail: bixj@ihep.ac.cn

1) Due to the model-dependent nature of the neutrino flux measurement and the associated uncertainties, we cannot rule out the possibility that the DGE excess includes a minor hadronic component.

2) *Electrons* will denote both electrons and positrons hereafter if not specified.

Gaussian profile at large distances from the source. Many gamma-ray sources in the first LHAASO catalog are associated with pulsars, most of which could be PWNe or pulsar halos. Thus, the potential contamination of DGE by these sources is worth considering. We refer to all sources associated with pulsars as LHAASO PWNe/halos in this paper.

More intriguingly, the Galactic longitude profile of the DGE excess measured by LHAASO exhibits a correlation with some known gamma-ray sources that have large extensions, such as those in the Geminga and Cygnus regions. The significant increase in DGE around Geminga is likely due to signal leakage from the Geminga pulsar halo. For the Cygnus region, the measurement by LHAASO indicates that the bubble extends to at least 10° [15], while the size of the masked region at that location is 6°. Therefore, signals beyond 6° can contribute to the measurement of DGE.

In this paper, we introduce a novel approach to evaluate the contribution of leakage signals from LHAASO PWNe/halos to the TeV DGE excess based on the two-zone diffusion model of electrons. This perspective is entirely distinct from the previous attribution of the DGE excess to unresolved extended gamma-ray sources [7, 12, 16]. Additionally, we give an estimate of the signal leakage from the Cygnus bubble. In Section II, we introduce the two-zone diffusion model, as well as the measurements of LHAASO PWNe/halos in the first LHAASO catalog and the related pulsar characteristics. We adopt the two-zone diffusion model to fit the LHAASO measurements and then predict the signal leakage. Section III presents our results, including the Galactic longitude profile and gamma-ray energy spectrum contributed by the leakage signals. Section IV provides some extended discussions of the results, followed by a summary and outlook in Section V.

II. METHODS

The first LHAASO catalog of gamma-ray sources includes 90 sources, 35 of which are associated with pulsars. We assume these sources to be PWNe or pulsar halos. In the LHAASO catalog paper, their morphology is uniformly described using a Gaussian template [8]. While this approach effectively captures the signals near the pulsars, it may not accurately describe the gamma-ray signals at larger angular distances, considering the possible escape of the parent electrons from the central zone. In this study, we adopted a two-zone diffusion model to describe the gamma-ray surface brightness of these sources, ensuring that the central morphology of each source is in agreement with the LHAASO measurements. The leakage flux can then be estimated by extrapolating from the two-zone diffusion model.

A. Two-zone model

We assume that the electron propagation for the LHAASO PWNe/halos can be described by the diffusion-loss equation

$$\frac{\partial N(E_e,\boldsymbol{r},t)}{\partial t} = \nabla\cdot[D(E_e)\nabla N(E_e,\boldsymbol{r},t)] + \frac{\partial[b(E_e)N(E_e,\boldsymbol{r},t)]}{\partial E_e} + Q(E_e,\boldsymbol{r},t)\,, \quad (1)$$

where N is the differential electron number density at electron energy E_e, position $\boldsymbol{r}$, and time t. D is the diffusion coefficient, $b \equiv |\mathrm{d}E_e/\mathrm{d}t|$ is the energy-loss rate due to electromagnetic radiation, and Q is the source term.

The source is assumed to be point-like, and the electron injection rate is assumed to follow the time profile of the pulsar spin-down luminosity, i.e., $\propto (1+t/\tau)^{-2}$, where the spin-down time scale is set to be $\tau = 10$ kyr. The electron injection spectrum for each source is described in power-law form. Hence, the source injection function is expressed as

$$Q(E_e,\boldsymbol{r},t) = \begin{cases} q_0 E^{-\alpha}\delta\left(\boldsymbol{r}-\boldsymbol{r}_p\right)\left[\left(t_p+\tau\right)/(t+\tau)\right]^2, & t \geq 0 \\ 0, & t<0 \end{cases}, \quad (2)$$

where $\boldsymbol{r}_p$ is the position of the pulsar, decided by the pulsar distance d given in Table 1. t_p is the age of the pulsar, and $t=0$ corresponds to the birth time of the pulsar.

For the two-zone model, the diffusion coefficient takes the form

$$D(E_e,\boldsymbol{r}) = \begin{cases} D_1(E_e/100\ \mathrm{TeV})^{\delta}, & |\boldsymbol{r}-\boldsymbol{r}_p| < r_\star \\ D_2(E_e/100\ \mathrm{TeV})^{\delta}, & |\boldsymbol{r}-\boldsymbol{r}_p| \geq r_\star \end{cases} \quad (3)$$

where $r_\star$ is the size of the slow-diffusion zone, D_1 is the suppressed diffusion coefficient near the source, and D_2 is the typical diffusion coefficient of the Galaxy [17]. Both D_1 and D_2 are normalized at 100 TeV. The energy slope of the diffusion coefficient is assumed to be $\delta = 1/3$, as suggested by Kolmogorov's theory [18]. Unless specified, we take $D_1 = 4.5\times10^{27}$ cm^2 s^{-1}, as inferred from the surface brightness profile of the Geminga halo [19], and the size of the slow-diffusion zone to be $r_\star = 25$ pc.

For high-energy electrons ($E_e \gg 1$ GeV), energy losses are dominated by synchrotron radiation and inverse Compton scattering (ICS) [20], which is denoted as $b(E_e)$ in Equation 1. We use a 3 μG magnetic field to calculate the energy loss due to synchrotron radiation. For ICS, the Galactic interstellar radiation field (ISRF) is

Table 1. 1LHAASO sources associated with pulsars.

Name	RA/(°)	DEC/(°)	$N_0/(10^{-16}\mathrm{cm^{-2}s^{-1}TeV^{-1}})$	Γ	$\sigma/(°)$	Associated Pulsar	d /kpc	t_p/kyr	$\dot{E}/(\mathrm{erg\ s^{-1}})$
1LHAASO J0007+7303u	1.91	73.07	3.41 ± 0.27	3.4 ± 0.12	0.17 ± 0.03	PSR J0007+7303	1.4	14	4.50×10^{35}
1LHAASO J0216+4237u	34.1	42.63	0.18 ± 0.03	2.58 ± 0.17	$0.13^{\dagger}$	PSR J0218+4232	3.15	476000	2.40×10^{35}
1LHAASO J0249+6022	42.39	60.37	0.93 ± 0.09	3.82 ± 0.18	0.38 ± 0.08	PSR J0248+6021	2	62	2.10×10^{35}
1LHAASO J0359+5406	59.78	54.1	0.85 ± 0.06	3.84 ± 0.15	0.3 ± 0.04	PSR J0359+5414	3.8*	75	1.30×10^{36}
1LHAASO J0534+2200u	83.61	22.04	6.23 ± 0.1	3.19 ± 0.03	$0.06^{\dagger}$	PSR J0534+2200	2	1	4.50×10^{38}
1LHAASO J0542+2311u	85.71	23.2	2.93 ± 0.12	3.74 ± 0.09	0.98 ± 0.05	PSR J0543+2329	1.56*	253	4.10×10^{34}
1LHAASO J0622+3754	95.5	37.9	1.42 ± 0.07	3.68 ± 0.1	0.46 ± 0.03	PSR J0622+3749	1.6	208	2.70×10^{34}
1LHAASO J0631+1040	97.77	10.67	0.54 ± 0.06	3.33 ± 0.16	$0.3^{\dagger}$	PSR J0631+1037	2.1	44	1.70×10^{35}
1LHAASO J0634+1741u	98.57	17.69	4.42 ± 0.15	3.69 ± 0.06	0.89 ± 0.04	PSR J0633+1746	0.19	342	3.30×10^{34}
1LHAASO J0635+0619	98.76	6.33	0.94 ± 0.1	3.67 ± 0.18	0.6 ± 0.07	PSR J0633+0632	1.35	59	1.20×10^{35}
1LHAASO J1740+0948u	265.03	9.81	0.41 ± 0.04	3.13 ± 0.15	$0.11^{\dagger}$	PSR J1740+1000	1.23	114	2.30×10^{35}
1LHAASO J1809-1918u	272.38	−19.3	9.46 ± 1.27	3.51 ± 0.26	$0.22^{\dagger}$	PSR J1809-1917	3.27	51	1.80×10^{36}
1LHAASO J1813-1245	273.36	−12.75	1.42 ± 0.27	3.66 ± 0.34	$0.31^{\dagger}$	PSR J1813-1245	2.63	43	6.20×10^{36}
1LHAASO J1825-1256u	276.44	−12.94	5.08 ± 0.42	3.33 ± 0.13	$0.2^{\dagger}$	PSR J1826-1256	1.55	14	3.60×10^{36}
1LHAASO J1825-1337u	276.45	−13.63	10.1 ± 0.61	3.28 ± 0.09	$0.18^{\dagger}$	PSR J1826-1334	3.61	21	2.80×10^{36}
1LHAASO J1837-0654u	279.31	−6.86	3.06 ± 0.21	3.7 ± 0.12	0.33 ± 0.04	PSR J1838-0655	6.6	23	5.60×10^{36}
1LHAASO J1839-0548u	279.79	−5.81	3.03 ± 0.2	3.24 ± 0.09	0.22 ± 0.02	PSR J1838-0537	2.3*	5	6.00×10^{36}
1LHAASO J1848-0001u	282.19	−0.02	1.64 ± 0.1	2.75 ± 0.07	$0.09^{\dagger}$	PSR J1849-0001	1.9*	43	9.80×10^{36}
1LHAASO J1857+0245	284.37	2.75	<0.32	−	0.24 ± 0.04	PSR J1856+0245	6.32	21	4.60×10^{36}
1LHAASO J1906+0712	286.56	7.2	<0.19	−	0.21 ± 0.05	PSR J1906+0722	1.73*	49	1.00×10^{36}
1LHAASO J1908+0615u	287.05	6.26	6.86 ± 0.16	2.82 ± 0.03	0.36 ± 0.01	PSR J1907+0602	2.37	20	2.80×10^{36}
1LHAASO J1912+1014u	288.38	10.5	1.52 ± 0.1	3.26 ± 0.11	0.5 ± 0.04	PSR J1913+1011	4.61	169	2.90×10^{36}
1LHAASO J1914+1150u	288.73	11.84	0.79 ± 0.06	3.41 ± 0.13	0.21 ± 0.04	PSR J1915+1150	14.01	116	5.40×10^{35}
1LHAASO J1928+1746u	292.17	17.89	0.72 ± 0.07	3.1 ± 0.12	$0.16^{\dagger}$	PSR J1928+1746	4.34	83	1.60×10^{36}
1LHAASO J1929+1846u	292.04	18.97	0.64 ± 0.06	3.11 ± 0.12	$0.21^{\dagger}$	PSR J1930+1852	7	3	1.20×10^{37}
1LHAASO J1954+2836u	298.55	28.6	0.42 ± 0.05	2.92 ± 0.14	$0.12^{\dagger}$	PSR J1954+2836	1.96	69	1.10×10^{36}
1LHAASO J1954+3253	298.63	32.88	<0.04	−	0.17 ± 0.03	PSR J1952+3252	3	107	3.70×10^{36}
1LHAASO J1959+2846u	299.78	28.78	0.84 ± 0.07	2.9 ± 0.1	0.29 ± 0.03	PSR J1958+2845	1.95	22	3.40×10^{35}
1LHAASO J2005+3415	301.81	33.87	0.56 ± 0.05	3.79 ± 0.21	0.33 ± 0.05	PSR J2004+3429	10.78	18	5.80×10^{35}
1LHAASO J2005+3050	301.45	30.85	0.46 ± 0.05	3.62 ± 0.21	0.27 ± 0.05	PSR J2006+3102	6.04	104	2.20×10^{35}
1LHAASO J2020+3649u	305.23	36.82	2.29 ± 0.09	3.31 ± 0.06	0.12 ± 0.02	PSR J2021+3651	1.8	17	3.40×10^{36}
1LHAASO J2028+3352	307.21	33.88	1.61 ± 0.19	3.38 ± 0.19	1.7 ± 0.23	PSR J2028+3332	0.91*	576	3.50×10^{34}
1LHAASO J2031+4127u	307.95	41.46	2.56 ± 0.08	3.45 ± 0.06	0.22 ± 0.01	PSR J2032+4127	1.33	201	1.50×10^{35}
1LHAASO J2228+6100u	337.01	61	4.76 ± 0.14	2.95 ± 0.04	0.35 ± 0.01	PSR J2229+6114	3	10	2.20×10^{37}
1LHAASO J2238+5900	339.54	59	2.03 ± 0.12	3.55 ± 0.09	0.43 ± 0.03	PSR J2238+5903	2.83	27	8.90×10^{35}

[1] The power-law shape is defined by $\mathrm{d}N/\mathrm{d}E_\gamma = N_0(E_\gamma/50\ \mathrm{TeV})^{-\Gamma}$. [2] The pulsar distances marked with $*$ are "pseudo distances" (see the text for the definition). [3] The Gaussian widths marked with † are the 95% statistical upper limits. [4] PSR is an abbreviation for *pulsar*.

composed of the cosmic microwave background, infrared emission, and optical emission. These components are described by gray body distributions with temperatures of 2.7 K, 20 K, and 5000 K and energy densities of 0.26 eV cm^{-3}, 0.3 eV cm^{-3}, and 0.3 eV cm^{-3}, respectively.

We use a finite volume numerical method to solve Equation 1 to obtain the electron density $N(E_e,\boldsymbol{r},t)$ [21]. Electrons produce gamma rays through ICS with the Galactic ISRF [22]. We then perform line-of-sight integration to obtain the gamma-ray surface brightness $S(\theta,E_\gamma)$ around pulsars, where θ is the angular distance from pulsars.

B. LHAASO PWNe/halos

Among these 35 LHAASO PWNe/halos, 32 have been significantly detected by LHAASO-KM2A and were utilized in this study, excluding the Crab nebula as it is a very young source with few expected escaping electrons. In the first LHAASO catalog, their morphologies are all described by the Gaussian template, where σ represents the Gaussian width or its the 95 % upper limit. Their energy spectra follow a power-law shape according to $\mathrm{d}N/\mathrm{d}E_\gamma = N_0(E_\gamma/50\,\mathrm{TeV})^{-\Gamma}$. The gamma-ray spectral parameters of the LHAASO sources and parameters of the associated pulsars are listed in Table 1. For most cases, the pulsar distance, characteristic age, and spin-down luminosity are taken from the ATNF catalog [23]. When the pulsar distance is not available in the ATNF catalog, we use the "pseudo distance" derived from the empirical relation between the pulsar gamma-ray luminosity and total spin-down power [24]. Specifically, PSR J1849-0001 currently lacks gamma-ray pulse measurements. We assume its distance to be the same as that of PSR J1954+2836, as these two pulsars have similar ages and Gaussian widths.

C. Fitting method

Based on the LHAASO measurements of the morphology and energy spectrum for each source, we can obtain the Gaussian profile at each energy point between 10 TeV and 1 PeV. Taking LHAASO J1825-1337u as an example, Fig. 1 shows the Gaussian morphology at $E_\gamma = 32$ TeV, convolved with the point spread function (PSF) of LHAASO-KM2A, where the PSF width is 0.3°. The blue shaded band represents the statistical error, assuming that the errors of each parameter are independent. To accurately reproduce the gamma-ray profile within the central zone and minimize the influence of uncertainties at large angular distances, we fit the two-zone diffusion model to the Gaussian template within the 2.5σ range, employing a chi-square fitting method as follows:

$$\chi^2 = \sum_i^n \left(\frac{S(\theta, E_\gamma) - S_G(\theta, E_\gamma)}{\sigma_G^i} \right)^2, \tag{4}$$

where i is the data sampling point, n is the total number of sampling points, and the angular distance between sampling points is 0.1°. $S_G(\theta, E_\gamma)$ is surface brightness predicted by the Gaussian profile, $S(\theta, E_\gamma)$ is surface brightness predicted by the two-zone diffusion model, and σ_G^i is the point error based on Gaussian profile error, which is adjusted according to the sample size n. The morphology derived from the two-zone diffusion model is also convolved with the same PSF. The free parameters in the fitting process are q_0 and α, as defined in Equation (2), which determine the normalization and spectral shape of the gamma-ray emission, respectively.

As shown in Fig. 1, when the gamma-ray profile calculated by the two-zone diffusion model is consistent with the LHAASO measurement within the central zone, the profile at lager angular distance is significantly higher than the Gaussian template. This discrepancy arises because electrons spread widely when they escape from the slow-diffusion zone. Consequently, there are still many residual signals even after masking a region of 2.5σ. Therefore, the leakage signals are expected to contribute a considerable portion to the DGE.

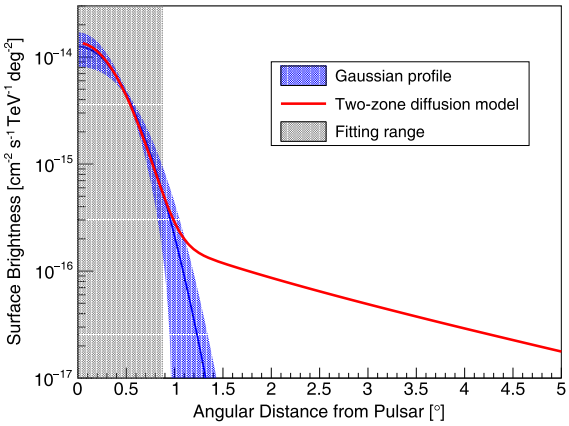

Fig. 1. (color online) Surface brightness profile of LHAASO J1825-1337u with $E_\gamma = 32$ TeV. The blue line represents the prediction of the Gaussian profile, with the corresponding shaded area indicating the error band, assuming the parameter errors are independent of each other. The red line represents the expectation from the two-zone diffusion model. The gray shaded area indicates the fitting range.

III. RESULTS

Using the model given by the fit introduced in Section II.C, we present the original and masked gamma-ray intensity maps in the Galactic plane in Fig. 2. The masking method employed is consistent with that used for the LHAASO DGE measurement. We can visually discern that considerable leakage signals remain in the Galactic plane, which should not be ignored compared to the measured DGE. In the default calculation, we assume $D_1 = 4.5\times10^{27}$ cm^2 s^{-1} and $r_\star = 25$ pc, as introduced in Section II.A. These two parameters cannot be constrained by the current measurements for each source, but they can affect the expected signal leakage. We discuss the influence of varying these parameters in Section IV.

It is worth noting that it is necessary to apply special treatments for the Cygnus and Geminga regions. In the region of Galactic longitude $70° - 90°$, there is an ultrahigh-energy gamma-ray bubble powered by a super PeVatron with an extension of $\sim 10°$, dubbed the "Cygnus bubble" [15]. However, in the LHAASO measurement of DGE, only a 6° radius circle is masked, leading to leakage of the bubble signals. The Cygnus bubble

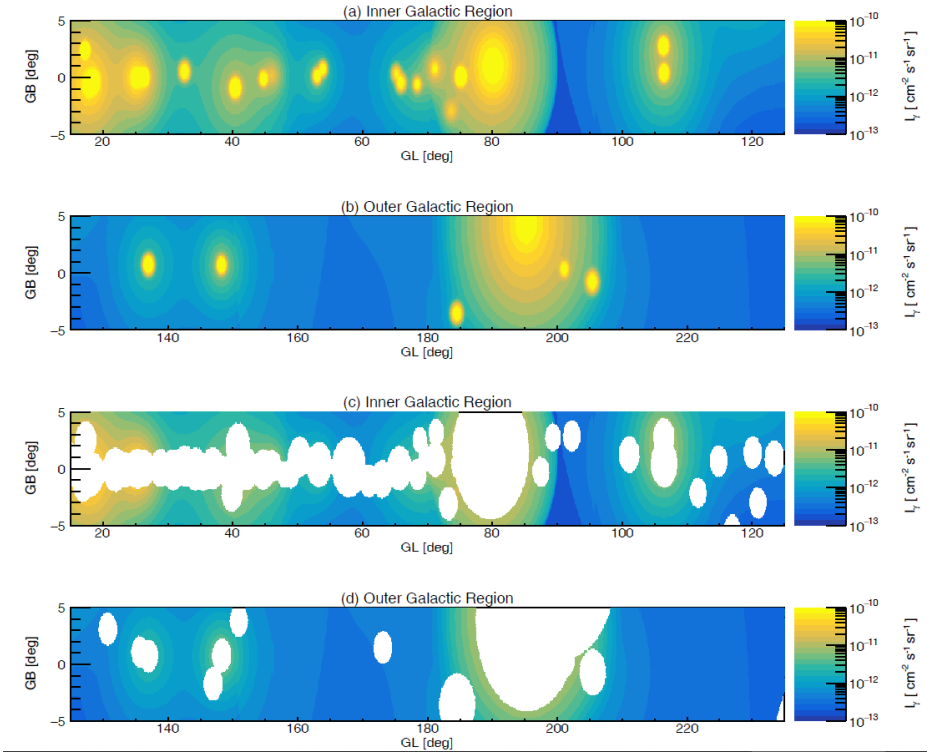

Fig. 2. (color online) Gamma-ray intensity map of Galactic plane contributed by LHAASO PWNe/halos and Cygnus bubble in energy range of 10−63 TeV. The signals from LHAASO PWNe/halos are modeled using a two-zone diffusion model. (a) Inner Galactic plane of $15^\circ < l < 125^\circ$. (b) Outer Galactic plane of $125^\circ < l < 235^\circ$. (c) Inner Galactic plane after masking the same region as the LHAASO DGE measurement. (d) Outer Galactic plane after masking the same region as the LHAASO DGE measurement. The white regions in (c) and (d) represent the masked regions.

most likely originates from hadronic interactions [15], and we straightforwardly use the LHAASO measurement to estimate the leakage flux in the range of $6^\circ - 10^\circ$ instead of using the prediction from the two-zone diffusion model. As the hadronic emission generated by the "cosmic-ray sea" is included in the LHAASO measurement of the Cygnus bubble, we have removed it to avoid redundant calculation.

At a Galactic longitude of approximately 190°, there is a remarkable excess coinciding with the location of the Geminga halo even after masking a radius of 8° around the Geminga pulsar. For the Geminga halo, we assume a slow-diffusion zone with $D_1 = 1.5 \times 10^{28}$ cm^2 s^{-1} and $r_\star = 50$ pc. The predicted leakage signals can reproduce this excess, and the assumed parameters are reasonable for the Geminga halo. The extension of Geminga observed in the significance map reported by LHAASO-KM2A [25] is larger compared to the measurements by HAWC [19], indicating a larger D_1. Besides, Ref. [14] pointed out that $r_\star$ should be larger than 30 pc to reproduce the surface brightness profile of the Geminga halo; otherwise, the profile would be too steep compared to the measurements.

Figure 3 shows the Galactic longitude profiles of DGE contributed by different components, including the CR-ISM interaction [12], and leakage signals of LHAASO PWNe/halos and Cygnus bubble in the energy bands of 10 – 63 TeV and 63 – 1000 TeV. The DGE measurement results significantly exceed the expectations of the CR-ISM interaction model. For the 10−63 TeV range, the DGE excess is primarily concentrated in four regions: (1) the region with $l \approx 20^\circ - 50^\circ$, (2) around the Cygnus bubble, (3) the region with $l \approx 100^\circ - 150^\circ$, and (4) around Geminga. Our signal leakage model significantly contributes to the excesses in regions (1), (2), and (4). For region (3), the signal leakage model can partly explain the excess (in $l \approx 100^\circ - 115^\circ$). For the 63−1000 TeV energy range, the excess primarily occurs in region (2), with a smaller amount coming from region (1). Our signal leakage model provides a good explanation for these excesses.

Interestingly, the DGE excess around Geminga is primarily observed in the 10 – 63 TeV energy range and is not significant in the 63 – 1000 TeV range. This observation coincides with the characteristics of the Geminga halo spectrum: the latest measurement by HAWC indicates that the gamma-ray spectrum of the Geminga halo exhibits an exponential cutoff at tens of TeV [26]. These phenomena favor the idea that the excess in this region originates from leakage signals of the Geminga halo

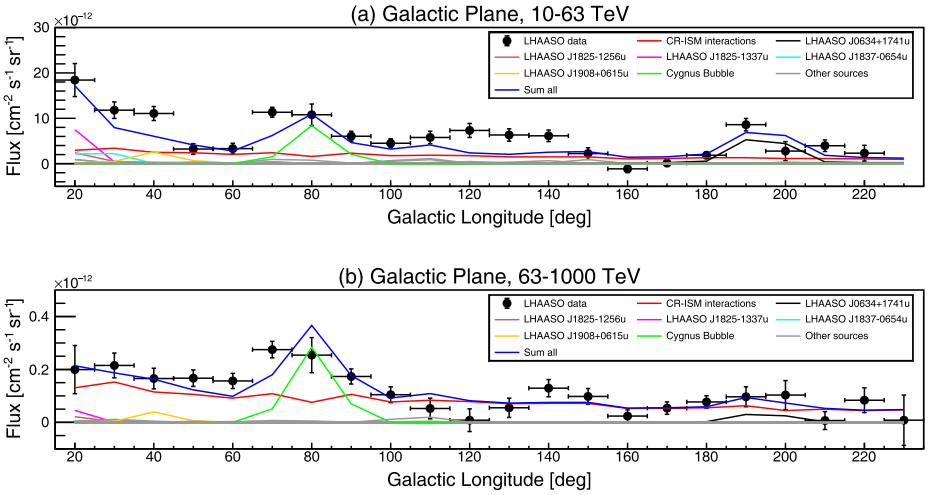

Fig. 3. (color online) Comparison of Galactic profiles of the diffuse emission and model. (a) In the energy range of $10-63$ TeV. (b) In the energy range of $63-1000$ TeV. The black points represent the measurements from LHAASO. The red line represents the prediction of the CR-ISM interaction model [12]. The blue line represents the sum of contributions from the CR-ISM interaction and leakage signals of the LHAASO PWNe/halos and Cygnus bubble. For sources with significant signal leakage, we have specifically marked their contributions to the DGE.

rather than other unresolved sources.

Figure 4 shows the gamma-ray spectra of DGE contributed by different components in the inner and outer Galactic plane. The total flux of DGE can be well explained once the signal leakage components are taken into account. In the inner Galactic plane region, for energies below 100 TeV, the DGE excess is predominantly contributed by the LHAASO PWNe/halos, while for energies above 100 TeV, it is mainly contributed by the Cygnus bubble. This is consistent with the constraint from the neutrino observation, which indicates that the DGE excess in $\approx 1-100$ TeV is dominated by leptonic components [12]. In the outer Galactic plane region, the DGE excess is contributed by leakage signals of LHAASO PWNe/halos, with no significant excess observed above 100 TeV. We note that the model still underestimates the DGE flux at ≈ 40 TeV for the case of the outer Galactic plane. This discrepancy is due to the underestimation in the longitude range of $l \approx 115^\circ - 150^\circ$, as shown in the top panel of Fig. 3.

IV. DISCUSSION

The uncertainties of the model arise from the parameters of the electron injection spectrum and electron propagation. The injection parameters (q_0 and α) are constrained by the LHAASO spectral measurements of the sources. The propagation parameters are mainly constrained by the morphology measurements of the sources; however, LHAASO currently provides only measurements of Gaussian extents for most sources, resulting in weaker constraints on the propagation parameters. Therefore, the uncertainties of the model primarily stem from the propagation parameters, especially D_1 and r_*, which determine the amount of signal leakage.

In the two-zone diffusion model, the slow-diffusion zone around a pulsar may originate from the turbulent environment created by the associated SNR [27]. Given that most of the pulsars listed in Table 1 are of the order of tens of kyr, it is reasonable to assume an average slow-diffusion zone scale of $r_\star = 25$ pc, which aligns with the expected scale of SNRs under typical parameters [28]. However, we still need to evaluate the impact of varying this value. Additionally, we should also consider the impact of the diffusion coefficient in the central zone, D_1, which may deviate from the value measured by HAWC [19]. Qualitatively speaking, the larger D_1 or smaller $r_\star$, the more easily electrons escape to distant regions, resulting in greater signal leakage. The specific impact of varying D_1 or $r_\star$ on the interpretation of the DGE excess is illustrated in Fig. 5.

We have demonstrated that the DGE excess in most regions can be interpreted by the signal leakage model under certain parameters, e.g., $D_1 \approx 5\times10^{27}$ cm^2 s^{-1} and $r_\star \approx 20-25$ pc. However, the gamma-ray flux predicted by the model is insufficient to match the data in the range of $l \approx 115^\circ - 150^\circ$, even when considering model uncertainties, as shown in Fig. 5. There are relatively few LHAASO PWNe/halos in this region, and the fluxes of LHAASO J0249+6022 and LHAASO J0359+5406 located in this region are relatively low. The excess gamma-ray emission in this region may be caused by some unresolved leptonic sources, such as indistinguishable halos. Therefore, the signal leakage from known sources and the contribution from unresolved sources should be considered complementary in explaining the DGE excess.

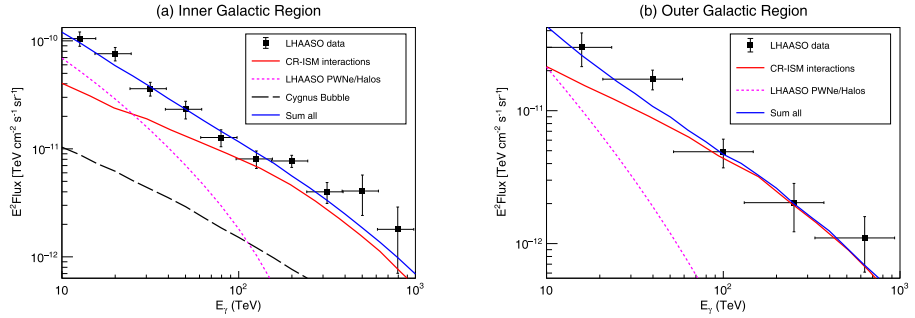

Fig. 4. (color online) Comparison of the measured DGE spectrum and model interpretation. (a) In the inner Galactic plane of $15° < l < 125°$. (b) In the the outer Galactic plane of $125° < l < 235°$. For each panel, the black points represent the LHAASO measurement. The solid red line represents the prediction of the CR-ISM interaction model [12], the dotted pink line represents the contribution from the leakage fluxes of LHAASO PWNe/Halo, and the black dashed line represents the leakage flux of Cygnus bubble. The blue line is the sum of all these components.

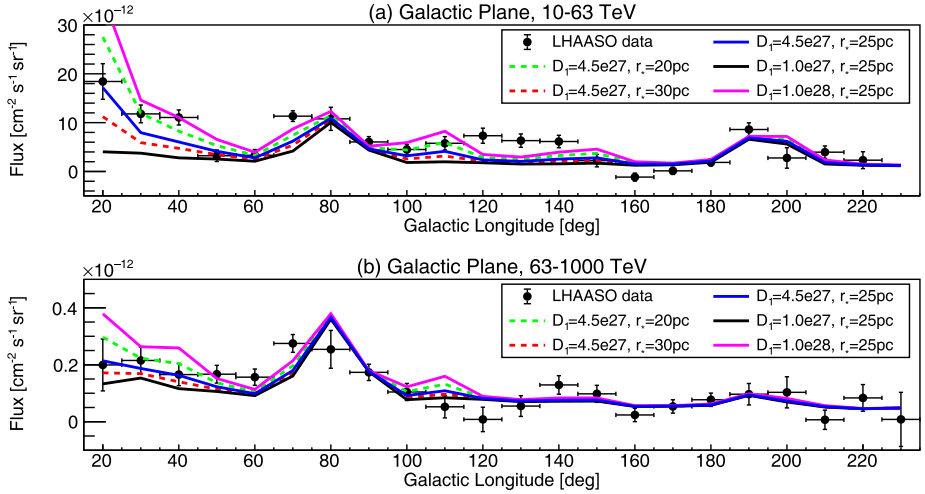

Fig. 5. (color online) Comparison of the Galactic longitude profiles of DGE by assuming different two-zone diffusion model parameters. (a) In the energy range of $10-63$ TeV. (b) In the energy range of $63-1000$ TeV. The lines represent the total contribution from the CR-ISM interaction, LHAASO PWNe/Halo, and Cygnus bubble. The units of D_1 are $\mathrm{cm}^2\ \mathrm{s}^{-1}$.

In this work, we predicted the large-angle signal leakage of LHAASO PWNe/halos using two-zone diffusion model for electrons. In fact, besides the two-zone diffusion model, other propagation models may also explain the surface brightness distribution around pulsars while predicting significantly higher gamma-ray signals at large angles compared to the Gaussian template. The superdiffusion model exhibits such characteristics, and previous works have discussed using the superdiffusion model to explain the morphology of pulsar halos [29, 30]. We expect that such models can achieve similar results to the two-zone diffusion model in interpreting the DGE excess.

We note that some studies on the joint analysis of the LHAASO diffuse gamma-ray measurement and IceCube neutrino measurement suggest a hadronic origin for DGE [31, 32]. It is crucial to emphasize that a consistent treatment of both datasets is essential for a robust joint analysis [12]. The neutrino flux measured by IceCube includes contributions from both the CR sea and hadronic point sources. To correlate the neutrino flux measured by IceCube with the diffuse gamma-ray data from LHAASO, the contributions from hadronic sources should be subtracted. Furthermore, the neutrino flux should be derived from the same region of interest as the LHAASO DGE analysis. If the same masking method used by LHAASO is not performed on the IceCube data, or if the contributions from hadronic point sources are not subtracted, it could lead to an overestimation of the neutrino flux, potentially resulting in the conclusion that the DGE excess has a hadronic origin.

V. CONCLUSIONS

The DGE excess phenomenon in the Galactic plane is generally believed to originate from unresolved sources with large extensions, such as pulsar halos. In this paper, we offered a new perspective to explain the DGE excess observed by LHAASO, suggesting that the large-angle

signal leakage from known sources could be a significant contributor to the DGE excess. As the excess predominantly originates from gamma rays produced by leptonic processes, we focused on possible PWNe and pulsar halos in the LHAASO source catalog. We first used the two-zone diffusion model to fit the central profile of the sources and get the extrapolated profile at large angular distances. Then, using the same masking method as in the DGE measurement, we determined the contribution from leakage signals of the LHAASO PWNe/halos to the DGE.

We demonstrated that the DGE excess in most regions of the Galactic plane can be well interpreted by the signal leakage model under certain parameters. Additionally, we showed that signal leakage from the Cygnus bubble must also be considered. We also note that in the Galactic longitude range of $l \approx 115^\circ - 150^\circ$, the gamma-ray flux predicted by our model is insufficient to match the observation, as there are few identified bright gamma-ray sources in that area. Unresolved extended sources may account for this discrepancy. Therefore, we emphasize that the signal leakage from known sources and the contribution from unresolved sources should be considered as complementary in explaining the DGE excess.

Besides the two-zone diffusion model, other propagation models, such as superdiffusion, could also explain the surface brightness distribution around pulsars while predicting significantly higher gamma-ray signals at large angles compared to the Gaussian template, which may similarly account for the DGE excess. As the LHAASO data continue to accumulate and with the advent of future high-resolution observations (e.g., LACT [33]), we will be able to provide more precise measurements of the morphology of known gamma-ray sources. This will allow us to place more stringent constraints on complex propagation models, such as the two-zone diffusion and superdiffusion models, thereby offering better insights into the origin of the DGE excess.

References

[1] A. W. Strong, I. V. Moskalenko, and V. S. Ptuskin, Ann. Rev. Nucl. Part. Sci. **57**, 285 (2007), arXiv: astro-ph/0701517

[2] M. Ackermann *et al.* (Fermi-LAT), Astrophys. J. **750**, 3 (2012), arXiv: 1202.4039[astro-ph.HE]

[3] R. Atkins *et al.* (Milagro), Phys. Rev. Lett. **95**, 251103 (2005), arXiv: astro-ph/0502303

[4] B. Bartoli *et al.* (ARGO-YBJ), Astrophys. J. **806**, 20 (2015), arXiv: 1507.06758[astro-ph.IM]

[5] M. Amenomori *et al.* (Tibet ASgamma Collaboration), Phys. Rev. Lett. **126**, 141101 (2021), arXiv: 2104.05181[astro-ph.HE]

[6] T. Prodanovic, B. D. Fields, and J. F. Beacom, Astropart. Phys. **27**, 10 (2007), arXiv: astro-ph/0603618

[7] T. Linden and B. J. Buckman, Phys. Rev. Lett. **120**, 121101 (2018), arXiv: 1707.01905[astro-ph.HE]

[8] Z. Cao *et al.* (LHAASO Collaboration), Astrophys. J. Suppl. **271**, 25 (2024), arXiv: 2305.17030[astro-ph.HE]

[9] Z. Cao *et al.* (LHAASO Collaboration), Phys. Rev. Lett. **131**, 151001 (2023), arXiv: 2305.05372[astro-ph.HE]

[10] R. Zhang, X. Huang, Z.-H. Xu *et al.*, Astrophys. J. **957**, 43 (2023), arXiv: 2305.06948[astro-ph.HE]

[11] R. Abbasi *et al.* (IceCube), Science **380**, adc9818 (2023), arXiv: 2307.04427[astro-ph.HE]

[12] K. Yan, R.-Y. Liu, R. Zhang *et al.*, Nature Astron. **8**, 628 (2024), arXiv: 2307.12363[astro-ph.HE]

[13] F.-W. Lu, Q.-G. Gao, and L. Zhang, Astrophys. J. **889**, 30 (2020)

[14] K. Fang, Phys. Rev. D **109**, 043041 (2024), arXiv: 2310.16594[astro-ph.HE]

[15] Z. Cao *et al.* (LHAASO Collaboration), Sci. Bull. **69**, 449 (2024), arXiv: 2310.10100[astro-ph.HE]

[16] A. Dekker, I. Holst, D. Hooper *et al.*, Phys. Rev. D **109**, 083026 (2024), arXiv: 2306.00051[astro-ph.HE]

[17] P.-X. Ma, Z.-H. Xu, Q. Yuan *et al.*, Front. Phys. (Beijing) **18**, 44301 (2023), arXiv: 2210.09205[astro-ph.HE]

[18] A. N. Kolmogorov, Proceedings: Mathematical and Physical Sciences **434**, 9 (1991)

[19] A. U. Abeysekara *et al.*, Science **358**, 911 (2017), arXiv: 1711.06223[astro-ph.HE]

[20] K. Fang, X.-J. Bi, S.-J. Lin *et al.*, Chin. Phys. Lett. **38**, 039801 (2021), arXiv: 2007.15601[astro-ph.HE]

[21] K. Fang, X.-J. Bi, P.-F. Yin *et al.*, Astrophys. J. **863**, 30 (2018), arXiv: 1803.02640[astro-ph.HE]

[22] G. R. Blumenthal and R. J. Gould, Rev. Mod. Phys. **42**, 237 (1970)

[23] R. N. Manchester, G. B. Hobbs, A. Teoh *et al.*, Astron. J. **129**, 1993 (2005), arXiv: astro-ph/0412641

[24] A. A. Abdo *et al.* (Fermi-LAT), Astrophys. J. Suppl. **187**, 460 (2010), arXiv: 0910.1608[astro-ph.HE]

[25] Y. Guo *et al.* (LHAASO Collaboration), PoS **ICRC2021**, 852 (2021)

[26] A. Albert *et al.* (HAWC Collaboration), PoS **ICRC2023**, 710 (2023)

[27] K. Fang, X.-J. Bi, and P.-F. Yin, Mon. Not. Roy. Astron. Soc. **488**, 4074 (2019), arXiv: 1903.06421[astro-ph.HE]

[28] D. A. Leahy and J. Williams, Astron. J. **153**, 239 (2017), arXiv: 1701.05942[astro-ph.HE]

[29] S.-H. Wang, K. Fang, X.-J. Bi *et al.*, Phys. Rev. D **103**, 063035 (2021), arXiv: 2101.01438[astro-ph.HE]

[30] K. Fang, S.-Q. Xi, and X.-J. Bi, Phys. Rev. D **104**, 103024 (2021), arXiv: 2107.02140[astro-ph.HE]

[31] K. Fang and K. Murase, Astrophys. J. Lett. **957**, L6 (2023), arXiv: 2307.02905[astro-ph.HE]

[32] C. Shao, S. Lin, and L. Yang, Phys. Rev. D **108**, L061305 (2023), arXiv: 2307.01038[astro-ph.HE]

[33] S. Zhang, PoS **ICRC2023**, 808 (2023)